Cerebral Cortex, January 2017;27: 863–876

doi:10.1093/cercor/bhv283
Advance Access Publication Date: 30 November 2015
Original Article

ORIGINAL ARTICLE

Deviant Processing in the Primary Somatosensory Cortex

Simon Musall[1,2,3], Florent Haiss[2,5,6], Bruno Weber[2,3] and Wolfger von der Behrens[2,4]

[1]Brain Research Institute, [2]Institute of Pharmacology and Toxicology, University of Zurich, Zurich, Switzerland, [3]Neuroscience Center Zurich, [4]Institute of Neuroinformatics, University of Zurich and ETH Zurich, Zurich, Switzerland, [5]Institute of Neuropathology and [6]Department of Ophthalmology, RWTH Aachen University, Aachen, Germany

Address correspondence to Wolfger von der Behrens, Institute of Neuroinformatics, University of Zurich and ETH Zurich, Winterthurerstrasse 190, CH-8057 Zurich, Switzerland. Email: wolfger@ini.uzh.ch

Abstract

Stimulus-specific adaptation (SSA) to repetitive stimulation has been proposed to separate behaviorally relevant features from a stream of continuous sensory information. However, the exact mechanisms giving rise to SSA and cortical deviance detection are not well understood. We therefore used an oddball paradigm and multicontact electrodes to characterize single-neuron and local field potential responses to various deviant stimuli across the rat somatosensory cortex. Changing different single-whisker stimulus features evoked robust SSA in individual cortical neurons over a wide range of stimulus repetition rates (0.25–80 Hz). Notably, SSA was weakest in the granular input layer and significantly stronger in the supra- and infragranular layers, suggesting that a major part of SSA is generated within cortex. Moreover, we found a small subset of neurons in the granular layer with a deviant-specific late response, occurring roughly 200 ms after stimulus offset. This late deviant response exhibited true-deviance detection properties that were not explained by depression of sensory inputs. Our results show that deviant responses are actively amplified within cortex and contain an additional late component that is sensitive for context-specific sensory deviations. This strongly implicates deviance detection as a feature of intracortical stimulus processing beyond simple sensory input depression.

Key words: local field potentials, mismatch negativity, sensory processing, single neurons, stimulus-specific adaptation

Introduction

The sensory environment is usually composed of many different sources, forming a complex scene that has to be structured by the nervous system in order to achieve efficient stimulus processing. A first step to reduce sensory input diversity is the reduction of neural responses to highly repetitive stimuli (Wark et al. 2007). Such adaptation of neural responses is an omnipresent feature in sensory systems and occurs at virtually all stages of the sensory pathway (Ohzawa et al. 1982; Khatri et al. 2004; Ganmor et al. 2010). A special case of adaptation is the so-called stimulus-specific adaptation (SSA) without a generalization towards other stimulus features (Ulanovsky et al. 2003; Katz et al. 2006; Hershenhoren et al. 2014). Here, sensory neurons selectively adapt to highly repetitive stimuli but retain their responsiveness to deviant stimulus features. Importantly, such deviant stimuli are not required to be of higher physical intensity to increase neural responses, as might be expected with general adaptation (Dudai 2004; Nelken and Ulanovsky 2007). SSA is thus a potential single-cell correlate of habituation (Netser et al. 2011; Gutfreund 2012). SSA has been observed in the auditory (von der Behrens et al. 2009; Farley et al. 2010; Taaseh et al. 2011; Hershenhoren et al. 2014) and visual system (Movshon and Lennie 1979; Müller

et al. 1999; Reches et al. 2010) as well as the somatosensory cortex (Katz et al. 2006). A common explanation for SSA is the conversion of stimulus-specific inputs onto a single sensory neuron (Katz et al. 2006; Nelken 2014). Repeated stimulation of one of these sensory channels reduces its transmission efficacy due to synaptic depression (Chung et al. 2002; Khatri et al. 2004; Katz et al. 2006) whereas the neuron still remains responsive to other synaptic inputs. In the neocortex, synaptic depression is particularly prominent at the thalamocortical synapse (Gil et al. 1999; Chung et al. 2002). Sensory adaptation is therefore more pronounced in cortex than in thalamus (Khatri et al. 2004; Katz et al. 2006), and depression of thalamocortical projections might be an important contributor to cortical SSA. Although this input depression model accounts for many aspects of SSA, deviant responses in cortex are even stronger than theoretically predicted (Taaseh et al. 2011), and it has been suggested that active deviance detection might be due to intracortical response modulation (Ulanovsky et al. 2003; Szymanski et al. 2009). However, significant SSA has also been observed at subcortical stages such as the auditory thalamus (Anderson et al. 2009; Antunes et al. 2010; Bäuerle et al. 2011) and the inferior colliculus (Malmierca et al. 2009; Ayala et al. 2012; Duque and Malmierca 2014).

A similar effect as in SSA is also seen in electroencephalographic (EEG) recordings in humans, showing an additional negative response to deviant stimulation, called mismatch-negativity (MMN) (Näätänen 1992, 2009). However, while SSA is commonly explained by input depression MMN is thought to reflect "true" deviance detection. Here, the repetitive pattern of a continuous stimulus sequence forms a prediction of future sensory events and the deviant-evoked MMN signals reflects a context-specific rule violation (Näätänen 1992; Todd et al. 2013). Whether SSA is a potential source of MMN is still under intensive debate (Nelken and Ulanovsky 2007; Sussman and Shafer 2014; Stefanics et al. 2014) and has been subject of numerous studies (Ulanovsky et al. 2003; Fishman and Steinschneider 2012; Harms et al. 2014; Klein et al. 2014).

In the present study, we sought to address if different stimulus features evoke SSA in primary somatosensory cortex (S1) and whether deviant responses could be actively enhanced by intracortical stimulus processing. We therefore performed electrophysiological recordings of single neurons and local field potentials (LFP) in S1 and used an oddball paradigm (Squires et al. 1975) to identify deviant-specific neural response patterns. We found robust SSA to several stimulus features that could be accurately predicted by a simple adaptation model using a set of 3 input parameters. To study intracortical deviant processing, we then applied spike and current-source density (CSD) analysis and found a distinct laminar response pattern that was specific for deviant stimulation. Furthermore, we observed an additional sensory response to deviant stimulation that occurred several hundred milliseconds after stimulus onset in a subset of neurons in the granular layer. In contrast to early responses, these late responses were lower in a many-standards control paradigm where deviant stimuli were presented with the same probability but in a different context than in the basic paradigm.

Materials and Methods

Animal Preparation

All experimental and surgical procedures were approved by the local veterinary authorities of the Canton Zurich, Switzerland, and carried out in accordance with the guidelines published in the European Communities Council Directive of November 24, 1986 (86/609/EEC). Seventeen adult female Sprague Dawley rats (233–360 g, Janvier) were used for this study. All rats were housed in groups of 3 with food and water ad libitum and an inverted 12:12-h light–dark regime. Acute experiments were performed under isoflurane in oxygen anesthesia combined with an analgesic (110 mg/kg Metamizol). While the surgery was performed under deep anesthesia (2–2.5% isoflurane), the anesthesia level for recording was kept as low as possible (usually 0.5–1.25% isoflurane). Anesthesia depth was monitored by breathing rate, eyelid reflexes, and absence of up- and down-states in the measured LFP signals.

Stimulation and Experimental Paradigms

The experimental control software was custom-written in LabVIEW (National Instruments) and generated an analog stimulation signal at 200 kHz and 16 bit. Single whiskers were placed in a glass capillary at a distance between the capillary tip and the whisker pad of 5 mm. The glass capillary was glued to a piezo-bending actuator (Piezo Systems) that was driven by a controller with a maximum output of 120V (Thorlabs). The stimulator and whisker movements were measured with a laser displacement sensor with 0.1 µm resolution (Micro-Epsilon). The stimulated whiskers were always contralateral to the recording side. In total, we used 5 different stimulation paradigms in order to characterize the cortical deviant responses in detail. The presentation sequence of the different paradigms in each experiment as well as the different blocks within one paradigm was fully randomized.

First, we applied a "whisker oddball" paradigm. Here, one whisker (either principal or adjacent whisker [AW]) was randomly assigned as the "standard", the other as "deviant". Subsequently, a stimulus sequence of 1000 deflections at 1 Hz was presented to the standard whisker. In 10% of the cases, the sequence was interrupted by a single deflection on the deviant whisker (deviant probability $P_{Dev} = 0.1$). After the first sequence and a 30-s break, the whisker identity of the deviant and standard whisker was swapped and a second sequence of 1000 deflections was presented. This "flip-flop" design corrects for potentially asymmetric responses to standard and deviant stimulation (Fig. 1C). Whisker deflections consisted of a single 120-Hz cosine wave (8.3 ms duration) with a deflection of 1.72° (300 µm) and a peak velocity of 648.8°/s.

Second, instead of switching the stimulated whisker, we exclusively changed the deflection velocity ("velocity oddball" paradigm). Here, only the principal whisker (PW) was stimulated with either a 120-Hz cosine wave (648.4°/s) or a 30-Hz cosine wave (161.1°/s) as standard and deviant. Again, the stimulus sequences were swapped in a flip-flop manner as described earlier.

In the third paradigm, we modulated the direction of the whisker deflection ("direction oddball" paradigm). Here, the PW was stimulated with a 120 Hz cosine wave of 324.2°/s velocity, and the deflection direction was either from caudal to rostral and back ($c > r$) or vice versa ($r > c$). Again, both features were randomly used as either standard or deviant and stimulated in a flip-flop configuration. For all results shown in Figures 1, 3, 4A–J, Supplementary Fig. 1, and Supplementary Fig. 3, P_{Dev} was set to 0.1, the repetition rate was 1 Hz, and 2 sequences of 1000 deflections each were presented.

Additionally, we measured these paradigms at different deviant probabilities (Figs 2D and 4K) and different repetition rates (Fig. 2A–C,E,F). Oddball effects at different deviant probabilities were measured at a 1 Hz repetition rate with either $P_{Dev} = 0.1$,

$P_{Dev} = 0.3$, or $P_{Dev} = 0.5$ for the whisker oddball paradigm. Oddball effects at different repetition rates were measured by varying the interstimulus intervals between 8 s (0.125 Hz) and 0.0125s (80 Hz) with $P_{Dev} = 0.1$. The number of presented stimuli was adjusted to keep the total protocol duration approximately constant at different rates. The number of stimulus presentations for different repetition rates were as follows: 0.125 Hz = 500, 0.25 Hz = 1000, 0.5 Hz = 2000, 1 Hz = 2000, 5 Hz = 4000, 10 Hz = 8000, 20 Hz = 16000, 40 Hz = 32000, and 80 Hz = 32000 stimuli. The velocity oddball paradigm and the direction oddball paradigm were only tested at repetition rates of 1 and 20 Hz.

A special case was the forth stimulus paradigm ("deviant alone"). Here, we used the same approach as in the oddball paradigms described earlier but the standard stimuli were omitted. Deviant-alone recordings were performed with repetition rates of 1 Hz and higher.

Finally, we tested in 5 animals if the increased deviant responses were due to true-deviance detection or could be explained by adaptation of specific sensory channels (Fig. 5). A possible way to address this question is by comparing deviant responses that are either embedded in a regular stimulus sequence (such as in the oddball paradigm where the highly probable standard stimulus provides regularity) or an irregular stimulus sequence that imposes the same adaptation load but without a single, highly probable regular standard stimulus. The regular sequence used here was the same as in the whisker oddball paradigm, but deviants were exclusively presented to the PW and standard stimuli to the AW. The repetition rate was 1 Hz, $P_{Dev} = 0.25$ and the standard probability $P_{st} = 0.75$. For the irregular sequence, we used a fifth paradigm called "many-standards." Here, we presented deviant stimuli to the PW but instead of stimulating a single AW with $P_{st} = 0.75$, standard stimuli were randomly distributed to all 3 AWs below the PW with the same probability of 0.25 per whisker (Fig. 5*B*). In the many-standards paradigm, the occurrence probability of each standard stimulus is therefore equal to the deviant stimulus.

Electrophysiological Recordings

Acute recordings were performed through an extracellular recording system (USB ME16/32-FAI, Multichannel Systems). The gain was 1200×; signals were digitized at 32 kHz and 16 bit. The reference electrode was a silver ball ventral to the craniotomy. In all experiments but the last (Fig. 5), we used a single shank, 16 contact linear electrode with 100 µm contact spacing and 177 μm^2 contact surface (Neuronexus) that was positioned in one barrel of the left cortex (Fig. 1*A*), identified through intrinsic optical imaging (usually C1 or D1, Fig. 1*B*) at 630 nm illumination (Grinvald et al. 1986). In 2 animals, 16 contact linear electrodes were implanted chronically and recordings were made repeatedly under anesthesia in both the left and (in a later recording session) the right barrel cortex. For recordings in the right barrel cortex, we stimulated the corresponding whiskers on the left side of the animals' snout. All recordings were performed within 1 week after electrode implantation.

We recorded the many-standards paradigm (Fig. 5) with a 4 shank, 32 contact linear electrode (8 contacts per shank) with a 200 µm contact spacing, and 177 μm^2 contact surface (Neuronexus). Electrodes were inserted at 100 µm/min until the last contact site reached the cortical surface which was covered with Ringer solution. The 2 chronically implanted animals mentioned earlier were also tested in the many-standards paradigm, and the resulting data were combined with the dataset from the acute recordings.

Electrophysiological Data Analysis

All data analysis was performed in Matlab (Mathworks). For spike detection, the signal was band-pass-filtered between 500–5000 Hz, and events that crossed a negative threshold of 6 standard deviations were counted as a spike. Single-unit (SU) activity was then isolated using the UltraMegaSort 2000 spike-sorting package (Hill et al. 2011). Spike waveforms were aligned, subjected to hierarchical k-means clustering, and subsequently aggregated into statistically distinct clusters. Each cluster was then evaluated manually for clear separability in amplitude and principal component space (Supplementary Fig. 1*C–E*). To consider a cluster as an SU, we required <0.5% refractory period violations and <5% missed spikes (estimated by a Gaussian-fit of the spike amplitude distribution). To ensure responsiveness to sensory stimulation, we used the Glass's Δ for stimulus-evoked spiking probability as a measure for each neurons signal-to-noise ratio (Stüttgen and Schwarz 2010). Glass's Δ was computed as follows:

$$\Delta = \frac{\text{mean}_{\text{Signal}} - \text{mean}_{\text{Baseline}}}{\text{SD}_{\text{Baseline}}}, \quad (1)$$

where $\text{mean}_{\text{Signal}}$ is the mean neural response within 20 ms after stimulus onset, $\text{mean}_{\text{Baseline}}$ the mean spontaneous activity 20 ms before the stimulus and $\text{SD}_{\text{Baseline}}$ the respective standard deviation. Firing probabilities were based on the peristimulus time histogram in response to the combined standard and deviant stimulation and we only included SUs with $\Delta > 2$. Glass's Δ was also used to identify neurons that exhibited a late sensory response. Here, we used the same approach as in Equation 1 but computed $\text{mean}_{\text{Signal}}$ as the average spiking activity between 100 and 400 ms after stimulus onset.

For LFP and CSD analysis, the continuously recorded signal was resampled at 1 kHz with an anti-aliasing finite impulse response filter implemented in Matlab. To compute CSDs, we used the inverse CSD method by Pettersen et al. (2006). We applied the spline iCSD method, which assumes a smoothly varying CSD between electrode contacts based on interpolation of a set of cubic polynomials. We assumed a homogeneous, isotropic conductivity of $\sigma = 0.3$ S/m within and directly above cortex (Pettersen et al. 2006). To reduce spatial noise, the estimated CSD was subsequently convolved with a Gaussian spatial filter with a standard deviation of 0.1 mm (Pettersen et al. 2006).

The data analysis was confined to responses elicited by the deviant and the directly preceding standard stimuli (Fig. 1*C*, indicated by black arrow). SSA-indices (SIs) were computed based on the averaged responses over all standards/deviants (100 for an oddball sequence of 1000 stimuli). For spikes, the mean response within a window from 0 to 20 ms after stimulus onset was used. In the whisker oddball paradigm with 80 Hz repetition rate, the window for spike analysis ranged from 0 to 12.5 ms. For the CSDs, the absolute of the lowest value between 0 and 20 ms after stimulus onset was used. When computing SIs for late sensory responses, we used spiking and CSD responses between 100 and 400 ms. SIs were computed by the following formula:

$$\text{SI} = \frac{(d(f_1) + d(f_2)) - (s(f_1) + s(f_2))}{d(f_1) + d(f_2) + s(f_1) + s(f_2)}, \quad (2)$$

$d(f_i)$ and $s(f_i)$ are responses to deviant or standard stimulation, respectively. f_i represents the stimulus feature, which was changed to induce an oddball effect. To compute SIs for each stimulus

feature separately, the above formula was modified to:

$$SI_1 = \frac{d(f_1) - s(f_1)}{d(f_1) + s(f_1)}, \quad (3)$$

$$SI_2 = \frac{d(f_2) - s(f_2)}{d(f_2) + s(f_2)}. \quad (4)$$

SI distributions were usually non-normal; we therefore report the median SIs and tested for significance against zero by using a Wilcoxon signed-rank test for zero median. For comparisons between distributions, a Wilcoxon rank-sum test was used. 95% confidence intervals were acquired by computing 1000 bootstraps based on the observed distribution statistics. To test for correlations between different variables, we used the Pearson correlation coefficient r. Boxplots in Figures 4 and 5 show the first and third quartiles, the inner line is the median, and notches show 95% CIs. Box whiskers represent minimum and maximum values, and crosses are outliers.

SSA Model

To model SSA changes at different repetition rates and deviant probabilities, we used a model based on the adaptation of responses to standard stimuli. Reduced response with increasing repetition rate was well described by a sigmoid fit function of the following form:

$$S_{St}(f) = r_{max} + \frac{(r_{min} - r_{max})}{1 + e^{-(\log(f * P_{st}) - x_{50})/v}}, \quad (5)$$

with v denoting the sigmoid slope, r_{max} and r_{min} the possible response range in Hz, x_{50} the inflection point, P_{st} the probability of a standard stimulus (normalized between 0 and 1, usually 0.9), and f the repetition rate in the oddball paradigm. Based on the achieved fit parameters, we predicted deviant responses by changing the stimulus probability to $P_{Dev} = 1 - P_{st}$ (usually 0.1). The resulting curve matched deviant-alone responses but overestimated response amplitude of deviants in the oddball paradigm. This mismatch between deviant and deviant-alone responses was then used to quantify the separation of different sensory channels that convey standard and deviant stimuli by introducing the additional term δ.

$$S_{Dev}(f) = r_{max} + \frac{(r_{min} - r_{max})}{1 + e^{-(\log(f * ((1 - 2P_{Dev}) * \delta + P_{Dev})) - x_{50})/v}}, \quad (6)$$

where $\delta = 1$ results in the same responses as with standard stimulation and $\delta = 0$ to responses with deviant-alone stimulation. To determine the optimal δ to describe deviant responses, we used nonlinear least squares regression. Based on the optimal δ, we then computed SI values based on the expected deviant and standard responses at each repetition rate or stimulus probability.

$$SI(f) = \frac{S_{Dev}(f) - S_{St}(f)}{S_{Dev}(f) + S_{St}(f)}. \quad (7)$$

Results

SSA in Rat Somatosensory Cortex

To assess whether deviant stimulation induces increased neural responses in somatosensory cortex, we simultaneously recorded single-unit (SU) and LFP responses in the rat barrel cortex with multielectrode arrays under isoflurane anesthesia (Fig. 1A). The electrophysiological recordings were done in individual barrels that were identified by using intrinsic optical imaging (Fig. 1B). The whisker oddball paradigm consisted of a 1-Hz sequence of short pulsatile whisker deflections that were applied to either the PW or an AW contralateral to the recording side. In 10% of all stimuli, the high-probability standard sequence (Fig. 1C, blue traces) was interrupted by a deviant stimulus, applied to the other whisker (red traces). Figure 1D shows the mean stimulus-evoked spiking responses over all recorded neurons to either PW or AW stimulation. As expected, responses to PW stimulation were stronger as with AW stimulation ($P = 0.013$). Clearly visible is also an increase in response amplitude with deviant presentation (red lines) compared with standard presentation (blue lines) that was most pronounced at the peak of the early onset responses (peak response differences: PW: 7.53 ± 6.32 Hz; AW: 10.40 ± 5.57 Hz, peak response latencies: PW: 10.17 ± 0.37 ms; AW: 10.51 ± 0.38 ms, mean ± s.e.m., $n = 76$ SUs). To quantify changes in response amplitude with deviant presentation, we computed a normalized SSA-index (SI, Equation 2). The SI ranges from –1 to 1 and negative values indicate a stronger response to standard and positive values to deviant stimuli. SIs were significantly positive over all neurons (Fig. 1E; signed-rank test, $P < 10^{-5}$), thus demonstrating robust SSA to whisker identity. The SI also controls for stimulus identity by integrating deviant and standard responses to stimulation of each whisker equally. Different responses to deviant and standard stimuli are therefore not solely explained by a particularly strong tuning towards a given whisker. Nevertheless, we sought to assess the impact of whisker tuning on the SI by computing the receptive field (RF) size as the absolute difference between PW and AW responses, divided by their sum. This metric is restricted between 0 and 1, with high values indicating particularly sharp tuning towards a single whisker. We found a positive correlation between SIs and RF size ($r = 0.351$, $P = 0.0017$), indicating that neurons with a sharp RF tend to have a higher SI as those that are more broadly tuned.

To test whether deviant responsiveness differs between the PW and AW in general, we also analyzed SIs for each whisker separately (Fig. 1F, Equations 3 and 4). Here, SIs were computed individually by comparing neural responses when both standard and deviant stimuli were presented to the adjacent ("AW", Y-axis) or the principal ("PW", X-axis) whisker. SIs were significantly positive for both PW and AW stimulation (median SI_{PW}: 0.10, signed-rank test, $P = 0.0183$; SI_{AW}: 0.08, $P = 0.0063$), demonstrating that SSA is also observed for each whisker individually. This further demonstrates that our results are not explained by overly strong tuning towards a single whisker (Antunes et al. 2010). Interestingly, we also found a significant inverse correlation between PW-SIs and AW-SIs ($r = –0.405$, $P = 0.0003$). This was most likely due to a specific tuning preference of individual cells to either the PW or AW. In fact, we found a positive correlation between PW-AW response differences and PW-SIs ($r = 0.463$, $P < 10^{-5}$), while being negatively correlated to AW-SIs ($r = –0.535$, $P < 10^{-5}$). In other words, cells that respond more strongly to PW over AW stimulation also exhibited higher PW-SIs whereas their AW-SIs were lower and vice versa.

We then tested whether SSA is similarly observed for other stimulus features. Here, stimulus sequences were exclusively applied to the PW and, instead of changing whisker identity, we applied a 1-Hz velocity oddball paradigm where the deflection velocity between standard and deviant stimuli was varied (Fig. 1G). Here, neural responses were stronger with high versus low-velocity stimulation ($P < 10^{-5}$). Deviant-induced responses were stronger than standard responses ($SI_{Velocity}$:

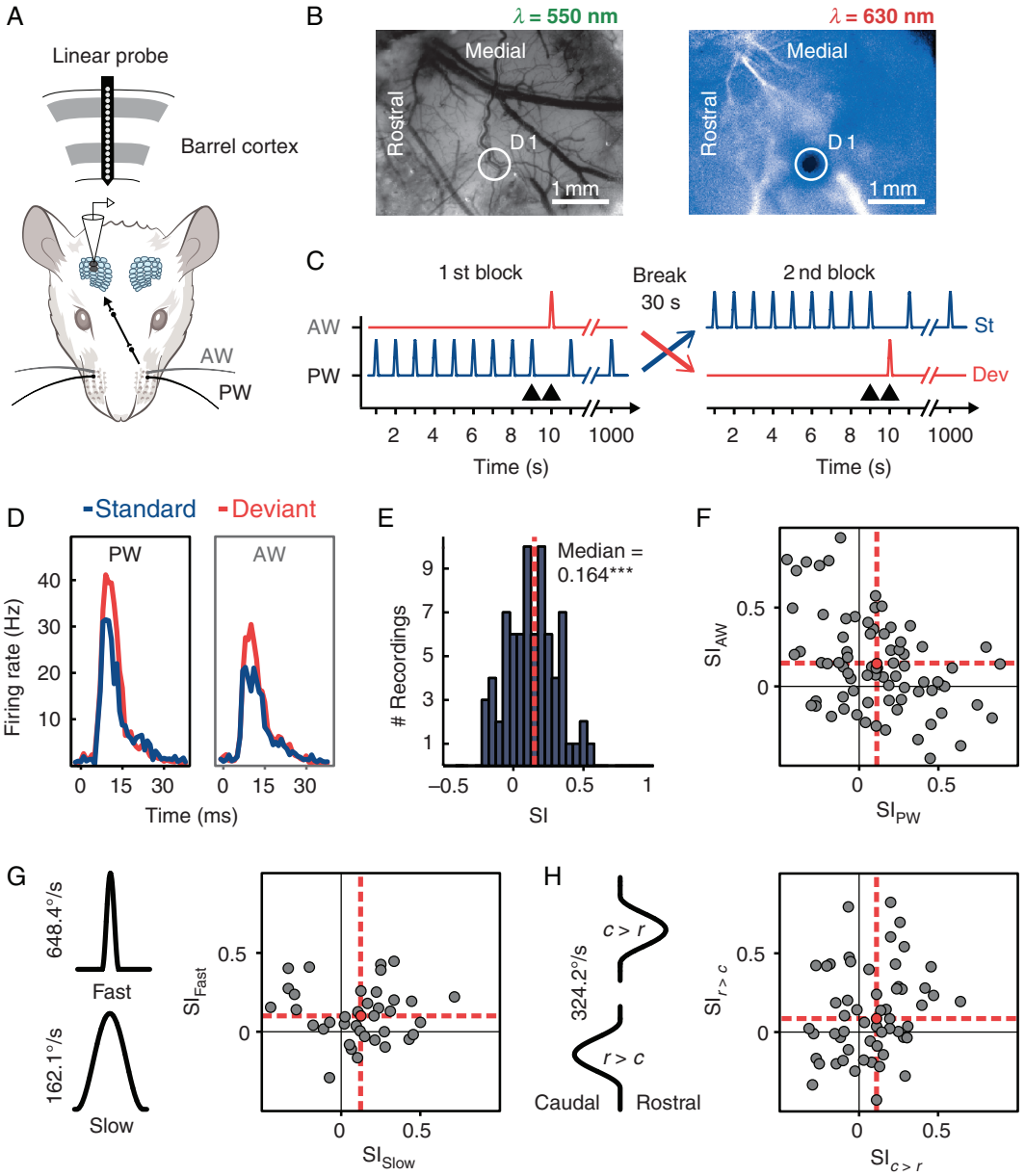

Figure 1. SSA to whisker identity, deflection velocity, and direction. (*A*) Recording and whisker stimulation. A linear electrode array was positioned in the barrel cortex, and pulsatile whisker deflections were applied to either the PW or the AW. (*B*) Identification of a single barrel using intrinsic optical imaging. The left panel shows the vessel pattern under green light. The right panel shows changes in red light absorption during D1 whisker stimulation. (*C*) Whisker oddball stimulation paradigm. During standard stimulation (blue trace), a 1-Hz stimulus sequence is applied to a single whisker (either AW or PW) and in 10% of all stimuli, a single deviant stimulus (red trace) is applied to the other whisker. After 1000 stimulus presentations and a 30-s break, the whiskers are swapped (second block). Black arrowheads indicate stimuli that were used for the analysis. Deviant and standard responses to each whisker were considered equally, thus controlling for a potential response bias towards a single whisker. (*D*) Averaged spiking response over all recorded neurons ($n = 76$) for either PW (left panel) or AW stimulation (right panel). Responses to standard stimulation are shown in blue, deviant responses in red. (*E*) Distribution of SI values from all SUs. The median SI was significantly positive ($P < 10^{-5}$). (*F*) SIs computed separately for standard and deviant stimulation of either the PW (*x*-axis) or AW (*y*-axis). Each circle denotes SIs of a single neuron; the red lines and dot indicate median values. (*G*) Velocity oddball stimulation paradigm. Pulses for either fast (upper left) or slow (lower left) whisker stimulation were applied to the PW at 1 Hz ($P_{Dev} = 0.1$). The scatter plot shows SIs for each deflection velocity separately. (*H*) Direction oddball paradigm. Pulses for either caudo-rostral (upper left, $c > r$) or rostro-caudal (lower left, $r > c$) whisker stimulation were applied to the PW at 1 Hz ($P_{Dev} = 0.1$). The scatter plot shows SIs for each deflection direction separately.

0.059, $P = 0.0002$, $n = 37$ SUs), and SSA was robust for both fast and slow whisker deflections (SI_{slow}: 0.125, $P = 0.019$; SI_{fast}: 0.1, $P = 0.0007$, see also Supplementary Fig. 1E). Similar effects were also observed when applying a 1-Hz direction oddball paradigm by changing whisker deflection direction from caudal to rostral and vice versa (Fig. 1*H* and Supplementary Fig. 1F, $SI_{Direction}$: 0.07, $P = 0.0013$; $SI_{c>r}$: 0.111, $P = 0.023$, $SI_{r>c}$: 0.084, $P = 0.0078$, $n = 55$ SUs). Here, we observed no significant difference in the response amplitude to each deflection direction ($P = 0.231$, Supplementary Fig 1F). The effect size for all 3 stimulus features was very similar with comparable studies that used oddball stimulation with pure tones and similar statistical properties (1 Hz repetition rate, $P_{Dev} = 0.1$) in the rat primary auditory cortex (von der Behrens et al. 2009; Taaseh et al. 2011).

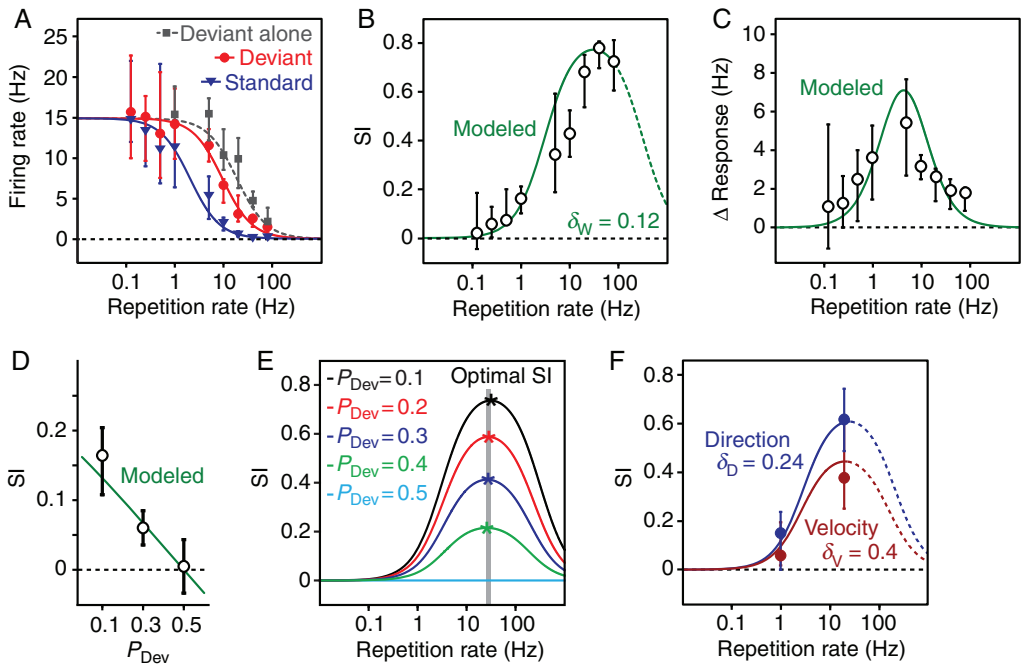

Figure 2. Modeling SSA based on oddball repetition rate, deviant probability, and input channel separation. (*A*) Neural responses to standard, deviant, or deviant-alone stimulation in the whisker oddball paradigm. Responses to standard stimuli were described by a sigmoidal fit function (blue curve) that also allowed predicting the course of deviant-alone responses (gray dashed curve). To accurately capture the response amplitudes of deviants embedded in an oddball sequence, the model was modified to quantify the amount of response separation between standard and deviant stimulation (red curve). Measured neural responses are shown as symbols for the standard (blue triangles), deviant (red dots), and deviant alone (gray squares). (*B*) Both measured (black circles) and modeled (green curve) SI values showed a steep increase for higher repetition rates. The dashed green curve shows predicted SIs for rates of >80 Hz. δ_W denotes the estimated response channel separation between neighboring whiskers. (*C*) Absolute differences between deviant and standard responses against repetition rate. The highest measured deviant-standard difference (black circles) was found at 5 Hz. This was in agreement with the model that predicted a peak absolute difference at 4.42 Hz (green curve). (*D*) Measured (black circles) and modeled SI values (green line) for different deviant probabilities at 1-Hz repetition rate. (*E*) Predicted changes in SI values for different deviant probabilities (P_{Dev}). As P_{Dev} increases, the predicted peak SIs (colored stars) are reduced and also slightly shift towards lower frequencies (gray bar). SIs remain at zero for $P_{Dev} = 0.5$ (light blue). (*F*) Measured (circles) and modeled (curves) SI values for either direction (blue) or velocity (red) deviants together with their respective δ_D and δ_V. Dashed lines show predicted SIs for frequencies of >20 Hz. Symbols show median values, error bars 95% CIs (*A–D,F*).

Importance of Repetition Rate, Deviant Probability, and Channel Separation

To assess whether SSA in somatosensory cortex may be explained by stimulus-specific input depression, we first focused on the relation between SSA and stimulus repetition rate. Synaptic depression is frequency dependent and increases with repetition rate (Chung et al. 2002; Khatri et al. 2004), which should therefore increase deviant-standard differences accordingly. Such a dependence of SSA on repetition rate has already been implicated by earlier studies in auditory cortex, but this relation was weak and only reported for a very narrow range between 0.5 and 3 Hz (Ulanovsky et al. 2003; Taaseh et al. 2011; Hershenhoren et al. 2014). In contrast, general adaptation in the somatosensory cortex extends over a wide frequency range and is markedly stronger for frequencies above 3 Hz (Khatri et al. 2004; Katz et al. 2006; Musall, von der Behrens, et al. 2014).

We therefore tested a wide range of repetition rates (0.125–80 Hz) and measured neural responses to standard and deviant stimuli in the whisker oddball paradigm with $P_{Dev} = 0.1$ (Fig. 2A). Standard responses (blue triangles) quickly decreased with frequency and reached a minimum for rates of 40 Hz and higher. The course of this amplitude reduction was well described by fitting a sigmoid function to the median responses over all units (Equation 5) with a neural response range between 14.93 and 0.06 Hz and an inflection point at a rate of 2.05 Hz. The function also included a parameter p to adjust the repetition rate to the probability of standard ($P_{st} = 0.9$) or deviant ($P_{Dev} = 0.1$) stimulation. Changing this parameter thus allowed us to compute expected deviant response amplitudes based on the same fit parameters that were obtained by standard stimulation. Predicted amplitudes (gray curve) matched well with measured deviant responses in the absence of standard stimuli ("Deviant alone", gray squares). However, deviant stimuli that were embedded in a standard sequence consistently evoked weaker neural responses (red circles) than with deviant-alone stimulation. Deviant responses were thus reduced by the presence of standard stimuli. In other words, if SSA is due to adaptation of specific sensory channels for PW and AW stimuli, these channels are not fully separate and stimulation of one will impose a certain "adaptation load" on the other channel. We therefore extended our basic model by an additional term δ to quantify such channel interactions, manifest in the adaptation of deviant responses (Equation 6). δ is restricted between zero (complete separation) and one (complete overlap), and we determined the optimal δ to match our recorded deviant responses (using otherwise the same fit variables as with standard data). The best fit (red curve) was found for a δ_W of 0.12, indicating that only a low sensory channel interaction has to be assumed to explain SSA to different whiskers with cortical response adaptation.

Based on the fitted standard and deviant response curves, we were then able to compute the expected SI values for different repetition rates (Equation 7) and compared these modeled and measured SIs (Fig. 2B). We recorded significantly positive SIs (black circles) even for very low repetition rates of 0.25 Hz ($P = 0.02$) and above ($P < 10^{-5}$). For 0.125 Hz, SIs were only

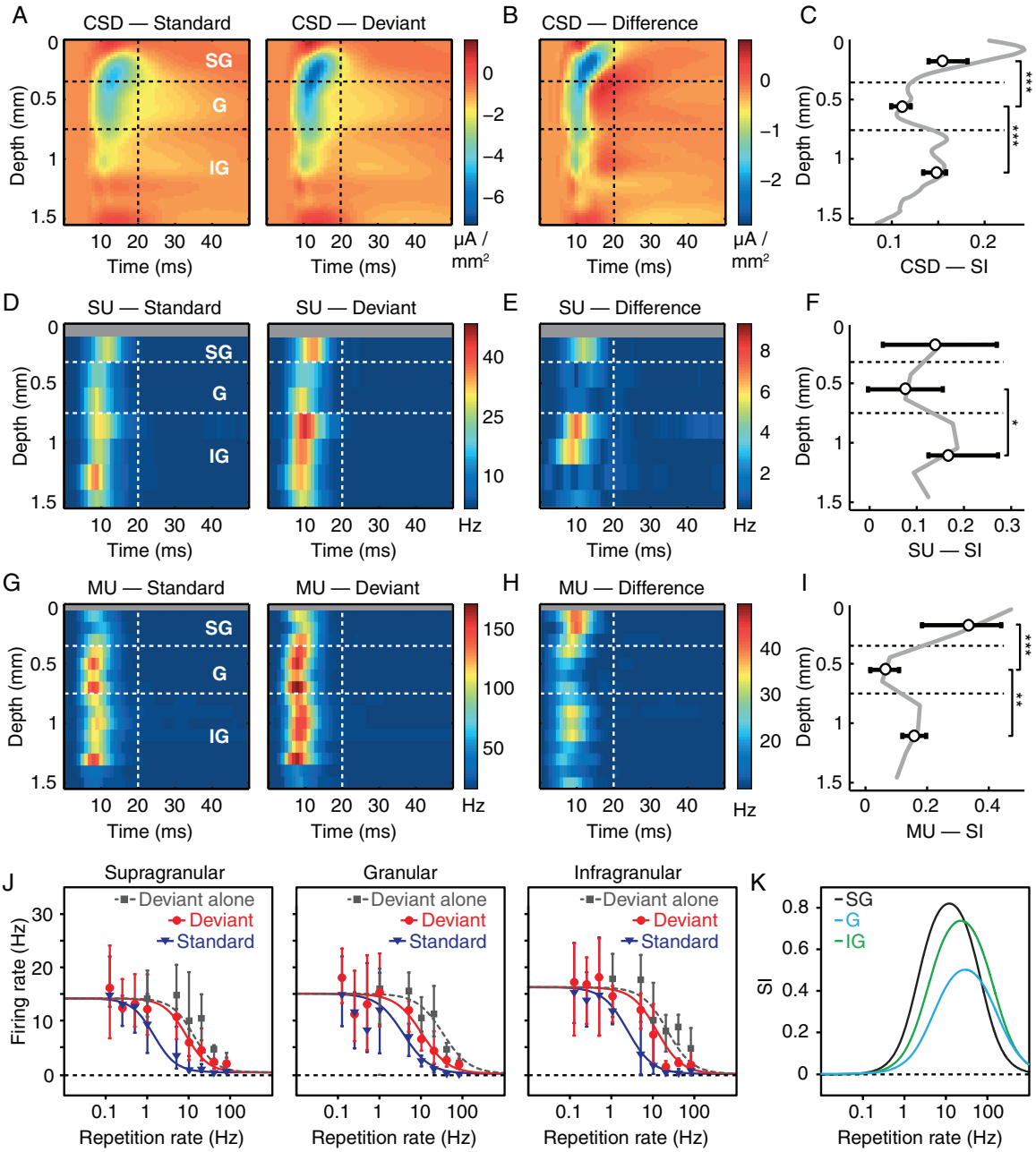

Figure 3. Layer-specific modulation of SSA in CSD and spike signals. (*A*) Averaged CSD responses over all recordings ($n = 14$ animals, 16 recording sessions) for either standard (left) or deviant stimulation (right) of the PW and AW in the whisker oddball paradigm. Repetition rate = 1 Hz, $P_{Dev} = 0.1$. Red colors indicate current sources, blue colors sinks. Dashed horizontal lines show borders of supragranular (SG), granular (G), and infragranular (IG) layers that were determined by the depth of the earliest detected current sinks (see also Supplementary Fig. 3A). Vertical dashed line indicates the end of the time window (starting at zero) that was used for computing SI values. (*B*) Absolute CSD differences between deviant and standard stimulation. Blue colors denote stronger current sinks with deviant stimulation. (*C*) CSD-based SI values against cortical depth. Gray line denotes the median SIs for different depths; black circles show median SIs for SG, G, and IG layers (***$P < 10^{-5}$, 95% CIs). (*D*) Averaged SU spike responses for all responsive neurons over all recordings ($n = 14$ animals, 76 SUs) for either standard (left) or deviant stimulation (right). Every row shows SU responses within 0.2 mm cortical depth. (*E*) Absolute SU spike differences between deviant and standard stimulation. (*F*) SU spike-based SIs values against cortical depth (*$P < 0.05$). (*G*) Averaged MU spiking responses for all responsive contacts over all recordings ($n = 14$ animals, 194 MUs) for either standard (left) or deviant stimulation (right). Every row shows MU responses within 0.1 mm cortical depth. (*H*) Absolute MU spiking differences between deviant and standard stimulation. (*I*) MU spiking-based SIs values against cortical depth (**$P < 0.01$). (*J*) Neural responses to standard, deviant and deviant-alone stimulation in the whisker oddball paradigm. Neural responses were analyzed for the SG (left panel), G (middle panel) and IG (right panel) layers, respectively and are shown as symbols for standard (blue triangles), deviant (red dots), and deviant alone (gray squares) stimulation. Sigmoidal fits were computed as described in Fig. 2A. (*K*) Modeled SI curves over different repetition rates for the SG (black), G (blue) and IG (green) layers.

significant for unsorted multiunit (MU) activity (median SI = 0.044, $P = 0.0048$) but not for single neurons ($P = 0.43$). Effect strength increased with repetition rate and achieved the highest SIs at 40 Hz. This was also confirmed by our model which predicted increasing SIs for rates above ~0.1 Hz and up to 30.91 Hz (solid green line). For even higher rates, SIs decreased again (dashed green line), suggesting an optimal frequency range at ~30 Hz where relative differences between standard

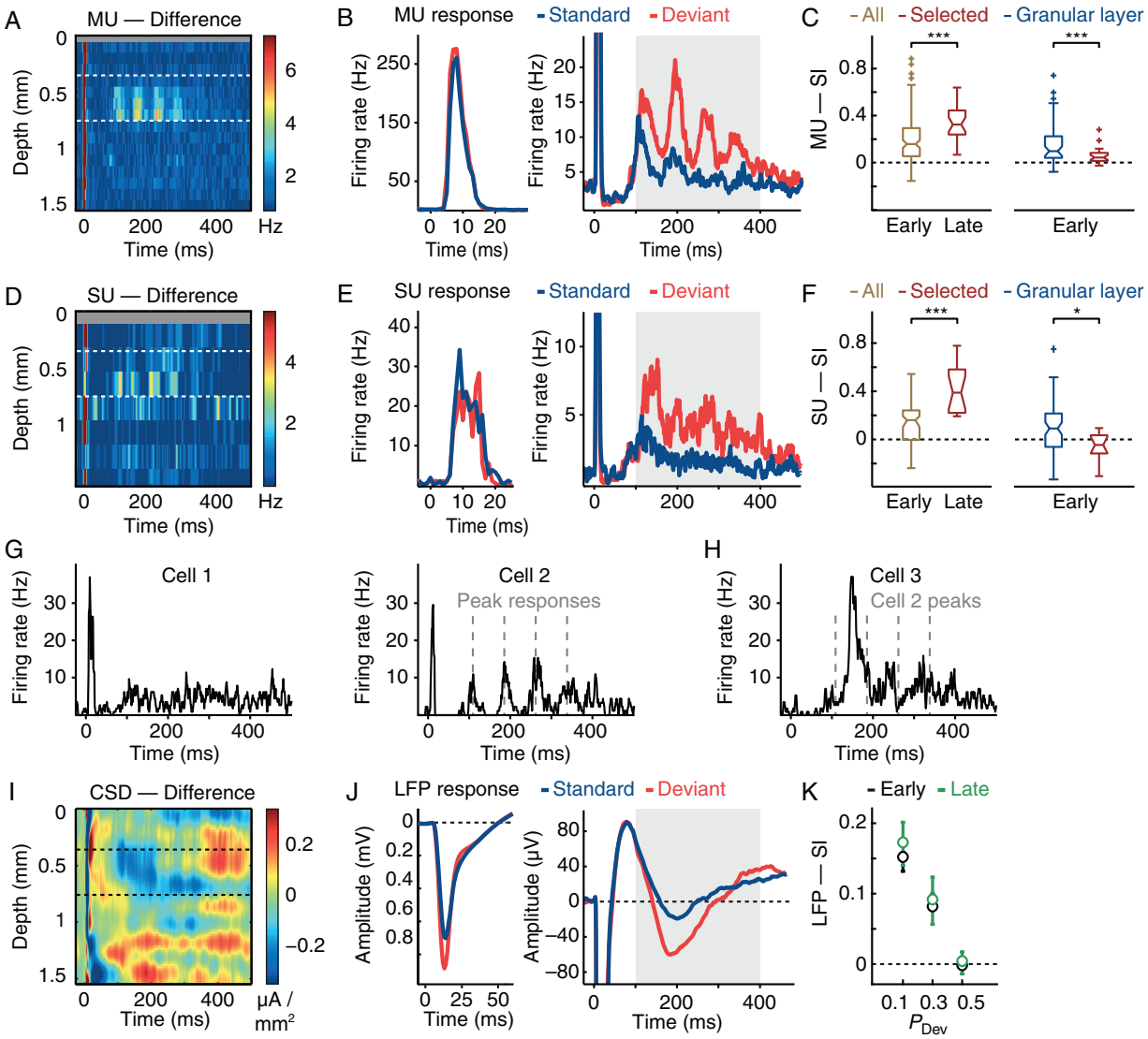

Figure 4. Deviant-specific late sensory response in the granular layer. (*A*) Absolute MU spiking differences between deviant and standard stimulation. Shown are the same MUs as in Figure 3*H* on a longer time scale ($n = 194$ MUs). (*B*) Averaged spiking response over all MUs that exhibited a second, long-latency deviant response ($n = 28$ MUs). The left panel shows the early sensory responses for standard (blue) or deviant (red) stimulation. The right panel shows the late sensory response with standard and deviant stimulation. Gray shading indicates the time window that was used for computation of late SIs. (*C*) Left panel: distribution of SIs over all MUs (yellow) and late SIs for selected units exhibiting a late response (red, $n = 28$ MUs). Right panel: distribution of SIs of the early response over all MUs in the granular layer (blue, $n = 79$ MUs) and all selected units with a late response (red). (*D*) Absolute SU spiking differences between deviant and standard stimulation. Shown are the same SUs as in Figure 3*E* on a longer time scale ($n = 76$ SUs). (*E*) Averaged spiking response over all SUs exhibiting a long-latency deviant response ($n = 9$ SUs). (*F*) Distribution of SIs over all SUs (yellow), late-responding SUs (red), and SUs in the granular layer (blue, $n = 39$ SUs). (*G*) Example traces for SUs with an early and late sensory response. While cell 1 shows a slow increase in spiking at longer latencies, cell 2 has a pronounced oscillatory response that starts after ~100 ms at intervals of ~75 ms (dashed lines). (*H*) Example traces for late-responding SUs without an early sensory response. Dashed lines indicate peaks for late responses of cell 2. Bursting activity of cell 3 precedes cell 2 bursting by ~15–30 ms. (*I*) Absolute CSD differences between deviant and standard stimulation. Blue colors denote stronger current sinks with deviant stimulation. (*J*) Averaged LFP response over all recording sites ($n = 14$ animals, 256 contacts). Differences between standard and deviant stimulation are clearly visible in both early and late sensory responses. (*K*) Median SIs based on early (black) and late (green) LFP responses for different deviant probabilities. Error bars show 95% CIs.

and deviant responses are highest. This was also true for absolute deviant-standard differences in firing rates although the peak difference was at a lower repetition rate of 4.42 Hz (Fig. 2*C*).

We then tested whether the model correctly predicts the impact of different deviant probabilities by performing additional experiments with $P_{Dev} = 0.3$ and 0.5. The latter is also a control condition as P_{Dev} and P_{st} are both 0.5 and SIs are thus expected to be zero. We found an almost linear decrease in SIs as P_{Dev} was increasing which was also well predicted by the model (Fig. 2*D*). The model showed a similar decrease when computing SIs for different P_{Dev} values over all repetition rates (Fig. 2*E* and Supplementary Fig. 2). Lastly, we sought to assess the sensory channel separation when changing whisker deflection velocity (δ_V) or direction (δ_D). As the basic course of adaptation was already known, only a small set of experimental data were required to estimate the difference between deviant and predicted "deviant alone" responses. We used recordings at 1 and 20 Hz and found higher sensory channel interaction for both velocity ($\delta_V = 0.4$, red) and direction ($\delta_D = 0.24$, blue) compared with different whisker channels ($\delta_w = 0.12$). For both modalities, the predicted SI curves also matched our measured results (Fig. 2*F*).

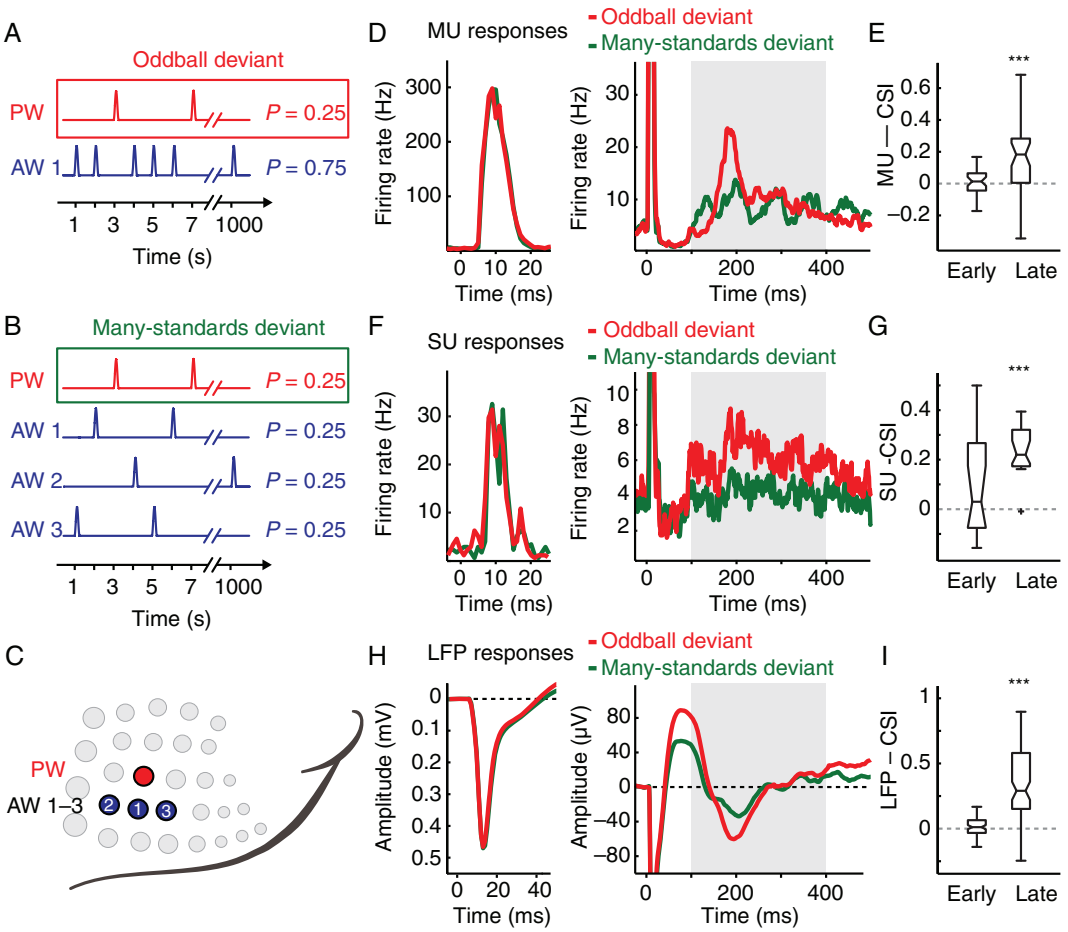

Figure 5. Late stimulus responses show true-deviance detection. (*A*) Illustration of the modified whisker oddball paradigm. Deviant stimuli were exclusively presented to the PW with a probability of 0.25 (red box); standard stimuli were presented to a single AW with a probability of 0.75 (blue trace). Deviant and standard whiskers were not swapped in a flip-flop manner. (*B*) Illustration of the many-standards paradigm. "Deviant" stimuli (green box) were delivered similarly as in *A* whereas standard stimuli were randomly distributed over 3 different AWs (blue traces). Hence, all whiskers were stimulated with the same probability of 0.25. (*C*) Illustration of the stimulated whiskers in the many-standards control. "Deviant" stimuli were always applied to the PW (red) and up to 3 AWs (blue) in the row below the PW were used for standard stimulation. (*D*) Averaged spiking response over all selected MUs that exhibited a second, long-latency deviant response ($n = 30$ MUs, 5 animals,). The left panel shows the early sensory responses to the oddball deviant (red) and many-standards deviant (green) stimulation. The right panel shows the late sensory response with a clear difference between both deviant types. Gray shading indicates the time window that was used for computation of late SIs. (*E*) Early MU CSIs were nondifferent from zero but late MU CSIs were significantly positive ($P < 10^{-5}$). (*F*) Averaged spiking response over all selected late-responding SUs ($n = 12$ SUs). (*G*) Late SU CSIs were significantly positive ($P = 0.0024$) whereas early SU CSIs were nondifferent from zero. (*H*) LFP early (left panel) and late (right panel) responses to deviant stimuli in the oddball and the many-standards paradigm over all recording sites ($n = 5$ animals, 160 contacts). (*I*) As with spiking, late LFP CSIs were significantly positive ($P < 10^{-5}$) whereas early LFP CSIs were not ($P = 0.193$).

SSA is Amplified in Supra- and Infragranular Layers of Cortex

The above results show that cortical SSA can be explained by stimulus-specific input depression when considering different degrees of sensory channel interaction for different stimulus features. Nevertheless, it is important to note that other mechanisms that were not considered in the model, such as intrinsic cellular properties or intracortical inhibition, may also significantly contribute to the generation of SSA. If SSA is mainly generated in subcortical areas or at the thalamocortical synapse, deviant stimuli should generate a stronger excitatory drive onto sensory cortex resulting in high response differences between deviant and standard stimulation, particularly in the cortical input layer IV. However, deviant-standard differences across different cortical layers should remain constant. Conversely, deviant-specific intracortical processing should be reflected in response differences that are variable between different cortical layers. To reveal the spatiotemporal structure of synaptic inputs to the barrel column, we therefore used CSD analysis, based on our LFP recordings in all cortical layers. As in earlier studies (Pettersen et al. 2006; Higley and Contreras 2007; Roy et al. 2011), we found a prominent, low-latency current sink between 0.35 and 0.75 mm of cortical depth that was most likely generated by thalamocortical inputs from the ventral posterior medial nucleus (VPM) into layer IV and lower layer III (Meyer et al. 2010). From here onward, we define this input range as the granular layer (Fig. 3, dashed lines "G"; see also Supplementary Fig. 3A) and all recordings above and below as supra- (SG) and infragranular (IG) layers, respectively. This response profile was observed for both standard and deviant stimulation in the whisker oddball paradigm (Fig. 3A, combined responses to PW and AW stimulation, repetition rate = 1 Hz, $P_{Dev} = 0.1$). The absolute differences between deviant and standard stimulation were most profound in the supragranular layers (Fig. 3B). CSD-based SIs were lowest in the granular layer (Fig. 3C, Wilcoxon rank-sum test, $P < 10^{-5}$) and showed 2

distinct peaks at ~50 µm and between 800 and 1100 µm cortical depth (gray line). Comparable results were also achieved in the velocity and direction oddball paradigm (Supplementary Fig. 3).

To analyze the laminar profile of SU responses, we combined SU responses for every 0.2 mm in cortical depth. Both standard and deviant stimulation evoked responses across all layers that were strongest in the infragranular layers (Fig. 3*D*). We also found pronounced response differences with deviant stimulation in the supra- and infragranular layers that were particularly low in the granular layer (Fig. 3*E*). A similar distribution was also seen in the SI analysis, showing that supra- and infragranular SIs were higher as in the granular layer, although this was only significant for the infragranular layers ($P = 0.63$ and 0.036, respectively; Fig. 3*F*). A potential reason for this difference to the CSD results is the low amount of recorded SUs in the supragranular layers ($n = 10$ versus 39 and 27 in the granular and infragranular layers, respectively). To increase the amount of neural signals, we therefore included all detected spikes instead of using only SUs. In the resulting MU data, we analyzed neural responses for every 0.1 mm cortical depth and observed the strongest responses in both the granular- and infragranular layers (Fig. 3*G*). As with SUs, the absolute response differences were strongest in the supra- and infragranular layers and remained low in the granular layer (Fig. 3*H*). This was clearly reflected in the SI analysis, showing that both supra- and infragranular SIs were significantly higher as in the granular layer (Fig. 3*I*, $P < 10^{-5}$ and 0.0091, respectively). Furthermore, the spatial profile of SI changes (gray line) also matched our results from the CSD analysis.

A potential reason for the weak SSA in the granular layers might be that granular neurons exhibit only little adaptation at low stimulation frequencies. We therefore compared SU responses to standard and deviant stimulation over all tested repetition rates for the SG, G, and IG layers separately. Here, standard responses showed comparable frequency-dependent adaptation between different layers (Fig. 3*J*, blue curves) whereas deviant-standard response differences were consistently lower in the granular layers (distance from blue to red curves). It thus seems that layer-specific differences in SSA are constant over a wide range of stimulus repetition rates. This was also seen when computing SI curves in all 3 depths over all frequencies (Fig. 3*K*).

We also tested whether differences in RF size may explain the observed differences in SSA across layers. We therefore computed the absolute response difference between PW and AW stimulation divided by their sum for the S, G, and IG layers. However, differences in RF size were small and remained insignificant between different layers (SG: 0.365 ± 0.081; G: 0.311 ± 0.04; IG: 0.352 ± 0.029; mean ± s.e.m., $n = 10$, 39, and 27 SUs; Wilcoxon rank-sum test: $P_{SG\text{-}G} = 0.51$, $P_{G\text{-}IG} = 0.401$, $P_{SG\text{-}IG} = 0.865$).

Taken together, these results suggest that increased response differences in the supra- and infragranular layers are not explained by thalamocortical input depression or layer-specific tuning properties and suggests that SSA is actively enhanced within the cortical circuitry.

Long-Latency Sensory Responses in the Granular Layer

Starting roughly 100 ms after stimulus onset, we observed a second difference in deviant-standard MU spiking responses in the 1-Hz whisker oddball paradigm (Fig. 4*A*). This later response was only observed in a subset of recordings (27 of 194 MUs, 8 of 14 animals) and mostly confined to the granular layer (23 of 79 MUs). A smaller subset was also seen in deeper layer V (4 of 84 MUs). Late responses were oscillatory and showed 3 to 4 peaks at intervals of ~70 ms (Fig. 4*B*, right). We could exclude that this was due to a mechanical artifact of the stimulator or stimulus-induced whisker movements during this time period by tracking the stimulator and resulting whisker movements (Supplementary Fig. 4). Interestingly, late responses were highly selective for deviant stimulation and SIs based on neural responses between 100 and 400 ms clearly exceeded SIs to early stimulus responses (Fig. 4*C* left panel, $P < 10^{-5}$). Furthermore, late-responding cells were only weakly deviant-selective in their early responses, compared with other cells in the granular layer (Fig. 4*C*, right panel, $P < 10^{-5}$). Similar results were also found when analyzing SU data (Fig. 4*D*–*F*). Here, 9 out of 76 SUs exhibited a late sensory response and were also mainly located in the granular layer (7 of 39 SUs) and to a lower extent in the deeper infragranular layers (2 of 27 SUs). Notably, the peak amplitude of late responses was closer to the initial onset response for SUs (~30% of early response amplitude), whereas the difference between early and late response amplitude was bigger in MUs (~7% of early response amplitude). This indicates that MU activity may obscure an objective assessment of late response amplitude because multiple neurons (of which presumably only a fraction exhibits a later response) are combined into a single MU cluster. Furthermore, late-responding SUs exhibited a variety of different response patterns to deviant stimulation. Some cells exhibited an initial stimulus response (Fig. 4*G*) and a second later response that was either slowly increasing after 100 ms (left panel) or occurring in defined bursts of activity (right panel, dashed lines). We also observed cells that exclusively responded at longer latencies at a markedly higher amplitude (Fig. 4*H*).

The spatial confinement to layer IV and partially deeper layer V suggests that these cells receive direct inputs from VPM (Meyer et al. 2010). However, the source of the deviant-specific late responses remained unclear. Probably, later sensory responses are also present in other cortical layers but remain insufficient to induce a spiking response. In this case, the spatial confinement of responsive cells might be because neurons in the granular layer are more excitable than other cortical neurons. To address this possibility, we checked for long-latency deviant-standard differences in the CSDs, which mostly reflect changes in the synaptic inputs to a neural population. As with spikes, long-latency differences in current sinks were weak but visible and showed a comparable spatiotemporal response profile (Fig. 4*I*). CSD differences were also visible after ~100 ms after stimulus onset and mainly confined to the granular layer, strongly suggesting that the layer specificity of later spiking responses is not due to differential neural excitability but specific synaptic input to layer IV.

SSA for the early and the late component was also found in the spatially less confined LFP signal where the later LFP response was an additional negative component with the same latency as in spiking and CSDs (Fig. 4*J*, right panel). Here, the deviant specificity of early and late responses was equally strong ($SI_{Early} = 0.142$, $SI_{Late} = 0.154$, $P = 0.502$, $n = 256$ contacts from all recording sites). We also observed a similar reduction in effect size when increasing deviant probability (Fig. 4*K*), which closely resembled our results from single neurons.

Long-Latency Responses Exhibit Context-Specific Deviance Detection

Lastly, we tested whether somatosensory cortex may also exhibit true-deviance detection properties, characterized by context-specific deviant responses that are not due to changes in stimulus probability. We therefore used an established protocol to test for context-dependent deviant responses in 2 different

stimulation paradigms (Jacobsen and Schröger 2001): The first one was the whisker oddball paradigm at 1 Hz and $P_{Dev} = 0.25$ with the exception that deviant stimuli were exclusively applied to the PW and not switched between PW and AW and (Fig. 5A). The whisker oddball paradigm provides a regular stimulus sequence where the high-probability standard stimulus ($P_{st} = 0.75$) allows establishing a rule and therefore a prediction of future stimuli. The violation of this rule by a deviant stimulus may then result in increased neural responses, constituting true-deviance detection. Conversely, standard stimuli in the many-standards paradigm were randomly distributed between 3 different AWs, resulting in the same presentation probability ($P = 0.25$) for each standard as well as the "deviant" stimulus (Fig. 5B). The "adaptation load" and stimulus presentation probability is therefore equal for deviants in either the whisker oddball or many-standards paradigm, but only oddball deviants may depict a specific-rule violation whereas no regularity is established in the many-standards paradigm. In agreement with the assumption of true-deviance detection, oddball deviants have been shown to produce stronger MMN than deviants in the many-standards paradigm (Todd et al. 2013).

For both paradigms, we presented deviant stimuli to the PW (usually C2) and standard stimuli to up to 3 different AWs in the row below the PW (Fig. 5C). Deviant stimulation in both the oddball and the many-standard paradigm evoked equally strong MU and SU response amplitudes at shorter latencies (Fig. 5D,F; left panels). In contrast, long-latency deviant responses in late-responding neurons were stronger in the whisker oddball compared with the many-standards paradigm (Fig. 5D,F; right panels). To quantify this effect, we computed a context-specificity index (CSI) by using the same formula as for the regular PW-SI (Equation 3), but instead of using deviant and standard responses, we compared responses with oddball and many-standard deviants. As shown in Figure 5 E,G, early CIs were non-different from zero for MU ($P = 0.235$) and SU responses ($P = 0.301$), whereas late CIs were significantly positive for both (MU: $P < 10^{-5}$, SU: $P = 0.0024$). A similar effect was also seen in the LFP (Fig. 5H,I). These results demonstrate that late responses are context-specific and not solely explained by stimulus probability.

Discussion

In the present study, we provide evidence for active deviance detection in the somatosensory cortex. Our adaptation model showed that early cortical responses can be explained by stimulus-specific input depression if different stimulus features are adjusted for the degree of sensory channel interaction. However, layer-specific CSD and spike analysis revealed that deviant responses markedly differ in different cortical layers, strongly implying that incoming deviant signals are further amplified within cortex. This is supported by the deviant-specific later responses that selectively appeared in a subset of cortical neurons and exhibited MMN-like true-deviance specificity.

SSA in Somatosensory Cortex

Our electrophysiological recordings demonstrate robust SSA of neurons in somatosensory cortex for deviations in whisker identity, deflection velocity, and direction. These results are widely comparable with a large body of literature that used the same experimental methodology in the auditory (Ulanovsky et al. 2003; von der Behrens et al. 2009; Antunes et al. 2010; Farley et al. 2010; Taaseh et al. 2011; Duque and Malmierca 2014; Hershenhoren et al. 2014) and visual system (Reches et al. 2010), further establishing SSA as a general feature of sensory processing. Somatosensory SSA had also been reported in an earlier study, showing that cortical responses to single-whisker stimulation are unaffected by prior stimulation of an AW (Katz et al. 2006). Here, the authors also found that neurons in the VPM are almost exclusively tuned to single whiskers and ultimately transmit this information in a one-to-one fashion to their corresponding cortical barrel. Consequently, cortical responses to multiple whiskers have been attributed to intracortical projections between individual barrels (Armstrong-James et al. 1991; Fox et al. 2003; Katz et al. 2006). However, our results show that adaptation to a neighboring whisker reduces neural responses to single-whisker stimulation (seen in the nonzero channel interaction δ_W; Fig. 2A,B). In line with other studies in somatosensory cortex (Kwegyir-Afful et al. 2005; Higley and Contreras 2007; Roy et al. 2011), we therefore argue that cortical AW responses are partially mediated by direct multiwhisker inputs from VPM. This notion also holds true for other stimulus features but their lower channel separation suggests that thalamocortical inputs for velocity and direction are less specifically tuned than for individual whiskers. This is in agreement with the rather broad tuning of thalamic neurons for deflection angle (Simons and Carvell 1989) and velocity (Pinto et al. 2000).

Intracortical Deviance Detection

Whisker stimulation induced robust neural responses throughout the cortex and the laminar CSD profile resembled earlier findings in barrel cortex (Pettersen et al. 2006; Higley and Contreras 2007; Roy et al. 2011). Interestingly, deviant stimulation induced layer-specific increases in neural response amplitude that were most pronounced in the supra- and infragranular layers. This was even more evident in the spatial profile of SI values that was highly comparable between spikes and CSDs. SIs were lowest in the granular and very deep (>1.25 mm) layers and showed a pronounced peak in the supragranular- and a second but weaker peak in the infragranular layers. The layer-specific SI increase in both CSDs and spiking shows that differential responses to standard and deviant stimulation are not just inherited by thalamic projections from VPM but actively amplified in the cortex. This is also indicated by consistent cortical SSA to 1-Hz stimulation whereas no adaptation at repetition rates below 12 Hz has been observed in either the VPM (Hartings et al. 2003; Khatri et al. 2004) or the trigeminal ganglion (Ganmor et al. 2010). Based on the input depression model, layer-specific changes in deviant responses could result from depression of cortical synapses as sensory responses propagate from the granular to the supra- and subsequently infragranular layers (Gilbert and Wiesel 1979; Douglas and Martin 2004). Assuming an increase in deviant responses through depression of cortico-cortical synapses, deviant responses should thus be most pronounced in the infragranular output layers. This might have also explained earlier results in auditory cortex where SIs were almost monotonically increasing with cortical depth (Szymanski et al. 2009). In contrast, we here found that deviant responses are strongest in the supragranular layers (Fig. 3). It thus seems that enhanced deviant representation is a specific feature of the intracortical circuitry and the respective processing layer. This is also indicated by the layer-specific adaptation during active whisking, where supragranular neurons show response depression whereas granular and infragranular responses are facilitated with repeated stimulation (Derdikman et al. 2006). The laminar profile of highest deviant responses also matches with projection targets from the nonlemniscal somatosensory thalamus (posteromedial

nucleus, POm) to cortical layers I and Va (Meyer et al. 2010). It is thus possible that interactions between cortex and POm are involved in enhancing cortical deviant responses. This would also relate well to several studies in the auditory system that showed that subcortical SSA is most prominent in the nonlemniscal pathway (Anderson et al. 2009; Antunes et al. 2010; Bäuerle et al. 2011).

A Deviant-Specific Late Sensory Response

We also found a second layer- and deviant-specific sensory response about 100 ms after stimulus presentation. Late somatosensory responses have also recently been described in the subthreshold membrane potentials of layer II/III neurons (Sachidhanandam et al. 2013). Here, late membrane potential fluctuations were only observed in mice that were trained in a stimulus detection task but not naive animals. Furthermore, optogenetic inhibition of late responses significantly reduced animal detection performance, demonstrating their importance for stimulus perception. Here, we show that long-latency spiking responses occur specifically in the granular layer, which may induce the observed subthreshold membrane fluctuations in layer II/III. Furthermore, the occurrence of late sensory responses under anesthesia shows that they at least partially represent a hardwired part of stimulus processing. Their long delay and deviant specificity indicate that late responses arise from intracortical network activity whereas the confinement of responses to layer IV and deeper layer V suggest that late responses may be driven by secondary VPM inputs. Potentially, such repeated recruitment of VPM neurons occurs downstream of cortical processing and is due to cortico-thalamic feedback. Earlier studies also showed that adaptation induces a shift in the balance between excitation and inhibition, resulting in increased neural excitability several hundred milliseconds after stimulus presentation (Malina et al. 2013). If deviant stimulation has a similar effect on the cortical excitation/inhibition balance, this might open a window of opportunity to evoke late sensory responses that can be modulated by feedback from downstream brain areas. In other words, late responses in layer IV may be due to changes in intracortical excitability but require feedback from higher-order brain areas to drive other cortical layers and induce a significant impact on perception. However, further studies are needed to elucidate the exact origin of late sensory responses and their relative importance for sensory perception in awake and behaving animals.

The existence of late sensory responses has also implications for understanding the physiological origins of MMN. MMN is characterized as a late, deviant-specific additional negative wave in EEG recordings, and several studies showed that SSA might be related but is not identical to MMN (Farley et al. 2010; Nelken 2014). Moreover, only few studies suggested that single neurons in A1 may exhibit context-specific deviant responses by showing that deviant responses in an oddball paradigm are stronger as theoretically predicted by the input depression model (Taaseh et al. 2011; Hershenhoren et al. 2014). In contrast, other studies found no evidence for context-specific deviance detection in A1 (Eriksson and Villa 2005; Farley et al. 2010). Our findings of early and late sensory responses in the same cortical neurons may aid to resolve this issue by demonstrating that deviant responses can be either dependent or independent of the presentation context, depending on their response latency. While both responses showed robust SSA in the oddball paradigm, only late deviant responses were significantly reduced in the many-standards control, demonstrating that they exhibit true MMN-like deviance detection. A potential interpretation of these results is that early responses are explained by SSA that solely depends on stimulus probability and might be due to input depression, whereas later deviant responses reflect context-specific true-deviance detection that may involve additional intracortical stimulus processing. However, the small percentage of late-responding neurons in S1 also raises the concern of whether our results could be the source of the rather large MMN that is observed in human EEG. A potential reason for this difference may be the fact that MMN is typically more pronounced in the temporal and frontal rather than primary sensory areas (Garrido et al. 2009). It is thus probable that the observed late responses are due to feedback from higher-order cortical areas that might give rise to the EEG signal that can be measured in humans. Also, despite their rare occurrence in individual neurons, we also found a clearly visible later response in the LFP, which integrates synchronous synaptic activity from a larger neural population as spike signals and is thus more comparable to the EEG (Musall, von Pföstl, et al. 2014). Indeed, the temporal profile of the late deviant-standard difference in the averaged LFP over all recording sites closely resembled MMN in human somatosensory cortex, although the extent of the observed response differences was lower (Strömmer et al. 2014). These similarities strongly suggest that late responses in S1 might be a physiological substrate for the generation of MMN, although it is likely that further intracortical processing in downstream areas is required to further amplify initial response differences. It would therefore be of particular interest to study properties of true-deviance detection in higher brain areas like S2 or the parietal cortex to identify additional components of the circuitry that is involved in the generation of MMN.

Supplementary Material

Supplementary material can be found at: http://www.cercor.oxfordjournals.org/.

Authors' contribution

B.W., W.B., and S.M. conceived and designed the study. S.M. and W.B. performed electrophysiological experiments. S.M. and W.B. analyzed the data. S.M., F.H., B.W., and W.B. wrote the manuscript.

Funding

This work was supported by the EU-FP7 program (BrainScales project 269921 to F.H.); the Swiss National Science Foundation (grant PP00B-110751/1 to B.W.); and SystemsX.ch (project 2008/2011-Neurochoice to B.W.).

Notes

We thank Fritjof Helmchen and Arko Ghosh for critically reading previous versions of the manuscript and valuable feedback. We thank Kevan Martin and the other members at the Institute of Neuroinformatics for their support. We thank Medartis AG for providing cortical screws for chronic implantations. *Conflict of Interest*: None declared.

References

Anderson LA, Christianson GB, Linden JF. 2009. Stimulus-specific adaptation occurs in the auditory thalamus. J Neurosci. 29:7359–7363.

Antunes FM, Nelken I, Covey E, Malmierca MS. 2010. Stimulus-specific adaptation in the auditory thalamus of the anesthetized rat. PLoS ONE. 5:e14071.

Armstrong-James M, Callahan CA, Friedman MA. 1991. Thalamocortical processing of vibrissal information in the rat. I. Intracortical origins of surround but not centre-receptive fields of layer IV neurones in the rat S1 barrel field cortex. J Comp Neurol. 303:193–210.

Ayala YA, Pérez-González D, Duque D, Nelken I, Malmierca MS. 2012. Frequency discrimination and stimulus deviance in the inferior colliculus and cochlear nucleus. Front Neural Circuits. 6:119.

Bäuerle P, von der Behrens W, Kössl M, Gaese BH. 2011. Stimulus-specific adaptation in the gerbil primary auditory thalamus is the result of a fast frequency-specific habituation and is regulated by the corticofugal system. J Neurosci. 31:9708–9722.

Chung S, Li X, Nelson SB. 2002. Short-term depression at thalamocortical synapses contributes to rapid adaptation of cortical sensory responses in vivo. Neuron. 34:437–446.

Derdikman D, Yu C, Haidarliu S, Bagdasarian K, Arieli A, Ahissar E. 2006. Layer-specific touch-dependent facilitation and depression in the somatosensory cortex during active whisking. J Neurosci. 26:9538–9547.

Douglas RJ, Martin KAC. 2004. Neuronal circuits of the neocortex. Annu Rev Neurosci. 27:419–451.

Dudai Y. 2004. Memory from A to Z: Keywords, concepts, and beyond. 1st ed. Oxford, UK: Oxford University Press.

Duque D, Malmierca MS. 2014. Stimulus-specific adaptation in the inferior colliculus of the mouse: anesthesia and spontaneous activity effects. Brain Struct Funct. 1–14.

Eriksson J, Villa AEP. 2005. Event-related potentials in an auditory oddball situation in the rat. BioSystems. 79:207–212.

Farley BJ, Quirk MC, Doherty JJ, Christian EP. 2010. Stimulus-specific adaptation in auditory cortex is an NMDA-independent process distinct from the sensory novelty encoded by the mismatch negativity. J Neurosci. 30:16475–16484.

Fishman YI, Steinschneider M. 2012. Searching for the mismatch negativity in primary auditory cortex of the awake monkey: deviance detection or stimulus specific adaptation? J Neurosci. 32:15747–15758.

Fox K, Wright N, Wallace H, Glazewski S. 2003. The origin of cortical surround receptive fields studied in the barrel cortex. J Neurosci. 23:8380–8391.

Ganmor E, Katz Y, Lampl I. 2010. Intensity-dependent adaptation of cortical and thalamic neurons is controlled by brainstem circuits of the sensory pathway. Neuron. 66:273–286.

Garrido MI, Kilner JM, Stephan KE, Friston KJ. 2009. The mismatch negativity: a review of underlying mechanisms. Clin Neurophysiol. 120:453–463.

Gilbert CD, Wiesel TN. 1979. Morphology and intracortical projections of functionally characterised neurones in the cat visual cortex. Nature. 280:120–125.

Gil Z, Connors BW, Amitai Y. 1999. Efficacy of thalamocortical and intracortical synaptic connections: Quanta, innervation, and reliability. Neuron. 23:385–397.

Grinvald A, Lieke E, Frostig RD, Gilbert CD, Wiesel TN. 1986. Functional architecture of cortex revealed by optical imaging of intrinsic signals. Nature. 324:361–364.

Gutfreund Y. 2012. Stimulus-specific adaptation, habituation and change detection in the gaze control system. Biol Cybern. 106:657–668.

Harms L, Fulham WR, Todd J, Budd TW, Hunter M, Meehan C, Penttonen M, Schall U, Zavitsanou K, Hodgson DM, et al. 2014. Mismatch negativity (MMN) in freely-moving rats with several experimental controls. PLoS ONE. 9:e110892.

Hartings JA, Temereanca S, Simons DJ. 2003. Processing of periodic whisker deflections by neurons in the ventroposterior medial and thalamic reticular nuclei. J Neurophysiol. 90:3087–3094.

Hershenhoren I, Taaseh N, Antunes FM, Nelken I. 2014. Intracellular correlates of stimulus-specific adaptation. J Neurosci. 34:3303–3319.

Higley MJ, Contreras D. 2007. Cellular mechanisms of suppressive interactions between somatosensory responses in vivo. J Neurophysiol. 97:647–658.

Hill DN, Mehta SB, Kleinfeld D. 2011. Quality metrics to accompany spike sorting of extracellular signals. J Neurosci. 31:8699–8705.

Jacobsen T, Schröger E. 2001. Is there pre-attentive memory-based comparison of pitch? Psychophysiology. 38:723–727.

Katz Y, Heiss JE, Lampl I. 2006. Cross-whisker adaptation of neurons in the rat barrel cortex. J Neurosci. 26:13363–13372.

Khatri V, Hartings JA, Simons DJ. 2004. Adaptation in thalamic barreloid and cortical barrel neurons to periodic whisker deflections varying in frequency and velocity. J Neurophysiol. 92:3244–3254.

Klein C, von der Behrens W, Gaese BH. 2014. Stimulus-specific adaptation in field potentials and neuronal responses to frequency-modulated tones in the primary auditory cortex. Brain Topogr. 27:599–610.

Kwegyir-Afful EE, Bruno RM, Simons DJ, Keller A. 2005. The role of thalamic inputs in surround receptive fields of barrel neurons. J Neurosci. 25:5926–5934.

Malina KC-K, Jubran M, Katz Y, Lampl I. 2013. Imbalance between excitation and inhibition in the somatosensory cortex produces postadaptation facilitation. J Neurosci. 33: 8463–8471.

Malmierca MS, Cristaudo S, Pérez-González D, Covey E. 2009. Stimulus-specific adaptation in the inferior colliculus of the anesthetized rat. J Neurosci. 29:5483–5493.

Meyer HS, Wimmer VC, Hemberger M, Bruno RM, de Kock CPJ, Frick A, Sakmann B, Helmstaedter M. 2010. Cell type–specific thalamic innervation in a column of rat Vibrissal Cortex. Cereb Cortex. 20:2287–2303.

Movshon JA, Lennie P. 1979. Pattern-selective adaptation in visual cortical neurones. Nature. 278:850–852.

Müller JR, Metha AB, Krauskopf J, Lennie P. 1999. Rapid adaptation in visual cortex to the structure of images. Science. 285:1405–1408.

Musall S, von der Behrens W, Mayrhofer JM, Weber B, Helmchen F, Haiss F. 2014. Tactile frequency discrimination is enhanced by circumventing neocortical adaptation. Nat Neurosci. 17:1567–1573.

Musall S, von Pföstl V, Rauch A, Logothetis NK, Whittingstall K. 2014. Effects of neural synchrony on surface EEG. Cereb Cortex. 24:1045–1053.

Näätänen R. 1992. Attention and Brain Function. Hove, UK: Psychology Press.

Näätänen R. 2009. Somatosensory mismatch negativity: a new clinical tool for developmental neurological research? Dev Med Child Neurol. 51:930–931.

Nelken I, Ulanovsky N. 2007. Mismatch negativity and stimulus-specific adaptation in animal models. J Psychophysiol. 21(3–4):214–223. doi:10.1027/0269-8803.21.34.214.

Nelken I. 2014. Stimulus-specific adaptation and deviance detection in the auditory system: experiments and models. Biol Cybern. 108(5):655–663.

Netser S, Zahar Y, Gutfreund Y. 2011. Stimulus-specific adaptation: can it be a neural correlate of behavioral habituation? J Neurosci. 31:17811–17820.

Ohzawa I, Sclar G, Freeman RD. 1982. Contrast gain control in the cat visual cortex. Nature. 298:266–268.

Pettersen KH, Devor A, Ulbert I, Dale AM, Einevoll GT. 2006. Current-source density estimation based on inversion of electrostatic forward solution: effects of finite extent of neuronal activity and conductivity discontinuities. J Neurosci Methods. 154:116–133.

Pinto DJ, Brumberg JC, Simons DJ. 2000. Circuit dynamics and coding strategies in rodent somatosensory cortex. J Neurophysiol. 83:1158–1166.

Reches A, Netser S, Gutfreund Y. 2010. Interactions between stimulus-specific adaptation and visual auditory integration in the forebrain of the barn owl. J Neurosci. 30: 6991–6998.

Roy NC, Bessaih T, Contreras D. 2011. Comprehensive mapping of whisker-evoked responses reveals broad, sharply tuned thalamocortical input to layer 4 of barrel cortex. J Neurophysiol. 105:2421–2437.

Sachidhanandam S, Sreenivasan V, Kyriakatos A, Kremer Y, Petersen CCH. 2013. Membrane potential correlates of sensory perception in mouse barrel cortex. Nat Neurosci. 16:1671–1677.

Simons DJ, Carvell GE. 1989. Thalamocortical response transformation in the rat vibrissa/barrel system. J Neurophysiol. 61:311–330.

Squires NK, Squires KC, Hillyard SA. 1975. Two varieties of long-latency positive waves evoked by unpredictable auditory stimuli in man. Electroencephalogr Clin Neurophysiol. 38:387–401.

Stefanics G, Kremláček J, Czigler I. 2014. Visual mismatch negativity: a predictive coding view. Front Hum Neurosci. 8:666.

Strömmer JM, Tarkka IM, Astikainen P. 2014. Somatosensory mismatch response in young and elderly adults. Front Aging Neurosci. 6:293.

Stüttgen MC, Schwarz C. 2010. Integration of vibrotactile signals for whisker-related perception in rats is governed by short time constants: comparison of neurometric and psychometric detection performance. J Neurosci. 30(6):2060–2069. doi:10.1523/JNEUROSCI.3943-09.2010.

Sussman ES, Shafer VL. 2014. New perspectives on the mismatch negativity (MMN) component: an evolving tool in cognitive neuroscience. Brain Topogr. 27:425–427.

Szymanski FD, Garcia-Lazaro JA, Schnupp JWH. 2009. Current source density profiles of stimulus-specific adaptation in rat auditory cortex. J Neurophys. 102:1483–1490.

Taaseh N, Yaron A, Nelken I. 2011. Stimulus-specific adaptation and deviance detection in the rat auditory cortex. PLoS ONE. 6:e23369.

Todd J, Harms L, Schall U, Michie PT. 2013. Mismatch negativity: translating the potential. Front Psychiatry. 4:171.

Ulanovsky N, Las L, Nelken I. 2003. Processing of low-probability sounds by cortical neurons. Nat Neurosci. 6:391–398.

von der Behrens W, Bäuerle P, Kössl M, Gaese BH. 2009. Correlating stimulus-specific adaptation of cortical neurons and local field potentials in the awake rat. J Neurosci. 29:13837–13849.

Wark B, Lundstrom BN, Fairhall A. 2007. Sensory adaptation. Curr Opin Neurobiol. 17:423–429.